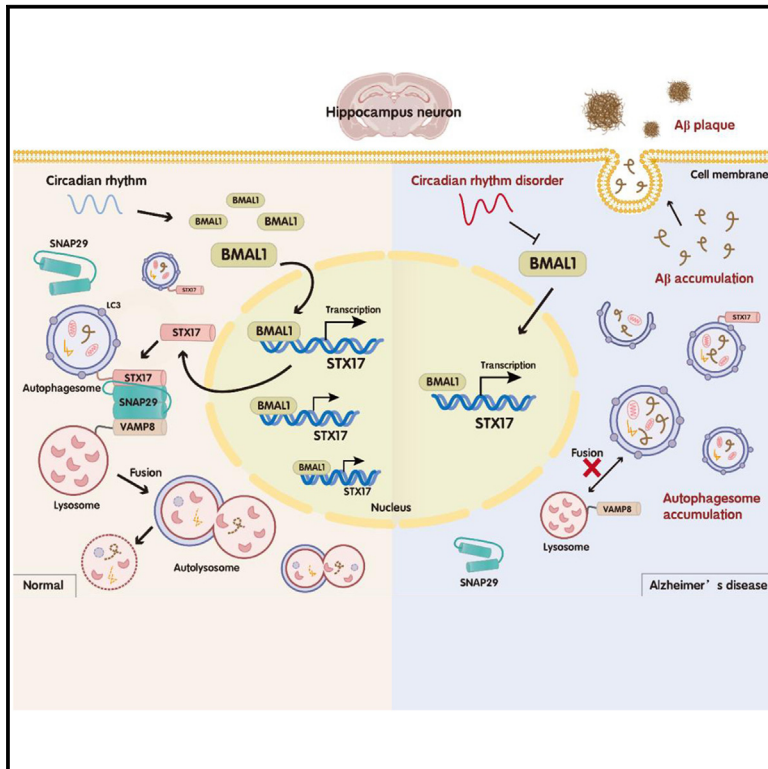# BMAL1 upregulates STX17 levels to promote autophagosome-lysosome fusion in hippocampal neurons to ameliorate Alzheimer's disease

## Graphical abstract



## Authors

Xiuya Zhou, Kaili Du, Tian Mao, ..., Ting Liu, Li Wang, Xiaohui Wang

## Correspondence

163.wangxh@163.com

## In brief

Neuroscience; Molecular neuroscience; Cellular neuroscience

## Highlights

- Reduced STX17 inhibits autophagy in hippocampal neurons, leading to Aβ accumulation

- BMAL1 enhances STX17 transcription, facilitating SNARE complex and Aβ clearance

- SNARE complex aids autophagy, clearing intracellular Aβ deposits

- Circadian rhythm disruption in early AD stages increases Aβ deposition

CellPress

# iScience

CellPress
OPEN ACCESS

## Article

# BMAL1 upregulates STX17 levels to promote autophagosome-lysosome fusion in hippocampal neurons to ameliorate Alzheimer's disease

Xiuya Zhou,[1,2] Kaili Du,[1,4] Tian Mao,[1] Ning Wang,[1] Lifei Zhang,[1] Yuan Tian,[1] Ting Liu,[1,4] Li Wang,[1,4] and Xiaohui Wang[1,3,4,5,*]

[1]Basic Medical Sciences Center, Shanxi Medical University, Taiyuan, China
[2]Department of Pathology, West China Hospital, West China Medical School, Sichuan University, Chengdu, China
[3]Key Laboratory of Cellular Physiology (Shanxi Medical University), Ministry of Education, Taiyuan, China
[4]Department of Pathology, Shanxi Medical University, Taiyuan, China
[5]Lead contact
*Correspondence: 163.wangxh@163.com
https://doi.org/10.1016/j.isci.2024.111413

## SUMMARY

We aim to investigate muscle ARNT-like protein 1 (BMAL1) regulation of syntaxin17 (STX17) in mouse hippocampal neurons, focusing on autophagy and amyloid-β (Aβ) deposition. Autophagosome-lysosome fusion in APP/PS1 hippocampal tissues was observed using transmission electron microscopy, while mRNA levels of LC3II and P62 were measured via reverse-transcription PCR (RT-PCR) after Amyloid precursor protein (APP) overexpression. STX17, linked to autophagy and differentially expressed in Alzheimer's disease (AD) brains, was knocked down or overexpressed to assess its effects. The results showed that reduced STX17 impairs autophagosome-lysosome fusion, leading to abnormal Aβ deposition. Coimmunoprecipitation (Co-IP) and immunofluorescence confirmed STX17 interaction with SNAP29 and VAMP8 to form SNARE complexes. Furthermore, BMAL1 binding to STX17 was examined using luciferase assays. Circadian rhythm disturbances and decreased BMAL1 expression in APP/PS1 mice were noted, while BMAL1 overexpression upregulated STX17 expression and promoted autophagy to reduce Aβ deposition. Thus, the BMAL1 protein can promote STX17 transcription to induce STX17-SNAP29-VAMP8 complex formation to clear intracellular Aβ through autophagy.

## INTRODUCTION

Alzheimer's disease (AD) is a neurodegenerative disease accounting for 50%–70% of all dementia cases.[1] The main pathological changes are Aβ acceleration and tau phosphorylation, which promote Neurofibrillary Tangle (NFT) formation in the cerebral cortex and hippocampus.[2] It is currently believed that Aβ aggregation plays a key role in the disease process of AD, and an imbalance between Aβ production and clearance is an important cause of the abnormal accumulation of Aβ.[3,4] In recent years, it has been believed that extracellular Aβ is the result of its toxic effect, and the accumulation of intracellular Aβ is the fundamental factor leading to cytotoxic effects.[5] Moreover, the Aβ clearance rate is significantly reduced during AD.[6,7] Autophagy, a key pathway for intracellular Aβ clearance, has important neuroprotective functions. When autophagosome transport is abnormal or lysosomes degrade autophagosome contents inefficiently, it leads to autophagosome accumulation and the formation of a large amount of Aβ.[8] The fusion of autophagosomes and lysosomes is an important part of autophagy.

Syntaxin 17 (STX17) can recruit soluble 29 kDa NSF attachment protein (SNAP29) and vesicle-associated membrane protein 8 (VAMP8) to the surface of lysosomes in the late stage of autophagy to form the SNARE complex, which promotes autophagosome-lysosome fusion.[9,10] There is evidence that adenovirus-mediated overexpression of STX17 in primary neurons can promote autophagosome-lysosomal fusion, which can reverse a significant retrovirus-induced increase in Aβ levels.[11] Knockdown of STX17 inhibits autophagosome-lysosomal fusion and affects axon growth in HT22 cells.[12] The aforementioned studies suggested that decreased expression of STX17 is an important factor that leads to autophagosome-lysosomal fusion dysfunction and causes Aβ deposition.

Studies have shown that circadian rhythm changes can directly exacerbate subsequent pathological changes in the early stage of AD.[13] The circadian system disturbance and sleep dysfunction in AD patients are characterized by highly fragmented sleep, sleep-wake dysfunction, and decreased daytime activity levels.[14–16] Accumulating evidence has demonstrated that long-term sleep restriction induces Aβ accumulation by disrupting the balance between Aβ production and clearance in rats.[17] 6-month-old APP/PS1 double-transgenic mice exhibited reduced sleep time, accompanied by the formation of amyloid plaques in the hippocampus and cortex.[18] The maintenance of

circadian rhythms relies on transcriptional/translational feedback loops (TTFLs) composed of circadian clock genes/proteins, which transport heterodimers formed by BMAL and Circadian Locomoter Output Cycles Kaput Protein (CLOCK) to activate the Period (PER) and Cryptochrome circadian clocks (CRYs).[19] In addition, other studies have shown that Aβ deposition and Bmal1 expression are decreased in the brains of 3xTg-AD mice,[20] and Bmal1$^{-/-}$ mice exhibit circadian rhythm disturbances in behavioral and molecular expression.[21] We also observed that Aβ induced a decrease in Bmal1 expression in HT22 cells,[22] which suggested that Bmal1 is crucial for the regulation of circadian rhythms in the AD model. STX17 is a clock-controlled gene (CCG) that is regulated by the Bmal1 signal output by the circadian rhythm downstream of the circadian gene.[23] However, the regulation of STX17 and autophagy by BMAL1 is unclear.

In this study, autophagosome-lysosome fusion and Aβ deposition were explored in AD models, such as APP/PS1 mice, and Amyloid precursor protein (APP) was overexpressed in HT22 cells. Furthermore, the causes of autophagosome-lysosome fusion dysfunction were observed through bioinformatics analysis, immunofluorescence (IF) colocalization, and coimmunoprecipitation (Co-IP). We found that the decrease in the expression of STX17 affected the formation of the STX17-SNAP29-VAMP8 complex, thereby inhibiting autophagosome-lysosome fusion. Crucially, we found that the circadian rhythm of APP/PS1 mice was disrupted in the early stage of AD and that the rhythm of Bmal1 expression was disrupted through wheel running. Moreover, it was further confirmed that Bmal1 can affect the transcription of STX17, thereby also suggesting that circadian rhythm affects autophagy in AD models, leading to abnormal Aβ deposition, which provides a new strategy for the treatment of AD.

## RESULTS

### Autophagosome-lysosome fusion disorders are observed in APP/PS1 mouse hippocampal tissue and APP-overexpressing HT22 cells

4-month-old and 8-month-old APP/PS1 mice as well as same-month-old wild-type (WT) mice were used to observe the expression of autophagy-related proteins. LC3II and P62 protein expression increased in the hippocampal neurons of APP/PS1 mice compared with those of WT mice, but LC3II and P62 protein upregulation was more obvious in 8-month-old APP/PS1 mice than in 4-month-old LC3II and P62 mice ($p < 0.05$) (Figure 1A). Reverse-transcription PCR (RT-PCR) revealed that LC3 mRNA levels also increased in 4-month-old and 8-month-old APP/PS1 mice ($p < 0.05$) (Figure 1B). Moreover, APP was overexpressed in HT22 cells by lentivirus (Figures 1C and 1D), and, compared to that in the control group and Lentivirus Negative Control (Lv-NC) group, the protein expression of LC3II and P62 in the Lentivirus Overexpression of Amyloid Precursor Protein (Lv-OE-APP) group significantly increased ($p < 0.05$) (Figure 1D). We also observed an increase in the number of endogenous LC3 puncta in the cytoplasm after APP was overexpressed ($p < 0.05$) (Figure 1E). These results suggested that autophagy is impaired in AD models.

To determine the reasons for autophagy impairment, transmission electron microscopy was used to observe the fusion of autophagosomes and lysosomes in the hippocampal neurons of 4-month-old mice. Autophagosomes obviously accumulated in the hippocampal neurons of 4-month-old APP/PS1 mice (shown by the double arrow); however, there were mainly autolysosomes in WT mice (indicated by the single arrows), and the number of autophagosome in APP/PS1 is more than that in WT group ($p < 0.05$) (Figure 1F). The aforementioned results demonstrated that autophagic flow was disrupted in hippocampal neurons in the early stages of AD, possibly because of impaired autophagosome-lysosome fusion. In our study, chloroquine was used as an autophagy inhibitor to block the autophagosome-lysosomal fusion process. The results showed that the protein expression of LC3II and P62 increased after the addition of chloroquine to the Lv-NC group ($p < 0.05$); however, there were no significant changes in the protein expression of LC3II or P62 in the Lv-OE-APP group after the addition of chloroquine (CQ) ($p > 0.05$) (Figure 1G). These findings suggested the occurrence of autophagosome-lysosome fusion disorders in HT22 cells after APP overexpression, which indicated that autophagy blockade in the AD model was caused by autophagosome-lysosome fusion disorders.

### Increased abnormal deposition of Aβ in APP/PS1 mouse hippocampal tissue and APP-overexpressing HT22 cells

Amyloid can be stained red by Congo red, which indicates pathological changes in amyloidosis. Congo red staining was used to observe the deposition of Aβ in the AD models. As shown, red amyloid deposits were observed in the hippocampal neurons of the APP/PS1 group (Figure 2A); at the same time, there were significant red deposits in the hippocampal neurons of the Lv-OE-APP group (Figure 2B) (indicated by the black arrows), suggesting that the abnormal deposition of Aβ increased in the AD models.

### Decreased expression of STX17 blocks the fusion of autophagosomes and lysosomes, resulting in abnormal deposition of Aβ in AD

The GEO: GSE21779 was analyzed to screen for significantly different genes in the brains of patients with AD according to $p < 0.05$ and $|logFC| \geq 1$. Moreover, the genes associated with AD significantly differed from the autophagy database genes and SNARE family genes; interestingly, the expression of STX17, which is associated with autophagy, significantly differed from that of AD in the SNARE family (Figure 3A). Gene Ontology (GO) and Kyoto Encyclopedia of Genes and Genomes (KEGG) pathway analyses revealed enrichment of pathways related to membrane fusion or adhesion (Figure 3B; Table S1), which showed that STX17 might play an important role in the autophagy process in AD. In addition, gene set enrichment analysis (GSEA) revealed that cellular functions were associated with autophagy and STX17 (Figure 3C; Table S2). RT-PCR and western blotting indicated that the expression of STX17 decreased ($p < 0.05$) (Figures 3D and 3E). IF showed that STX17 was mainly localized in the cytoplasm, and the fluorescence intensity of STX17 decreased after APP was overexpressed ($p < 0.05$) (Figure 3F).

To investigate whether STX17 can induce autophagy, we quantified autophagy levels via various methods. After small
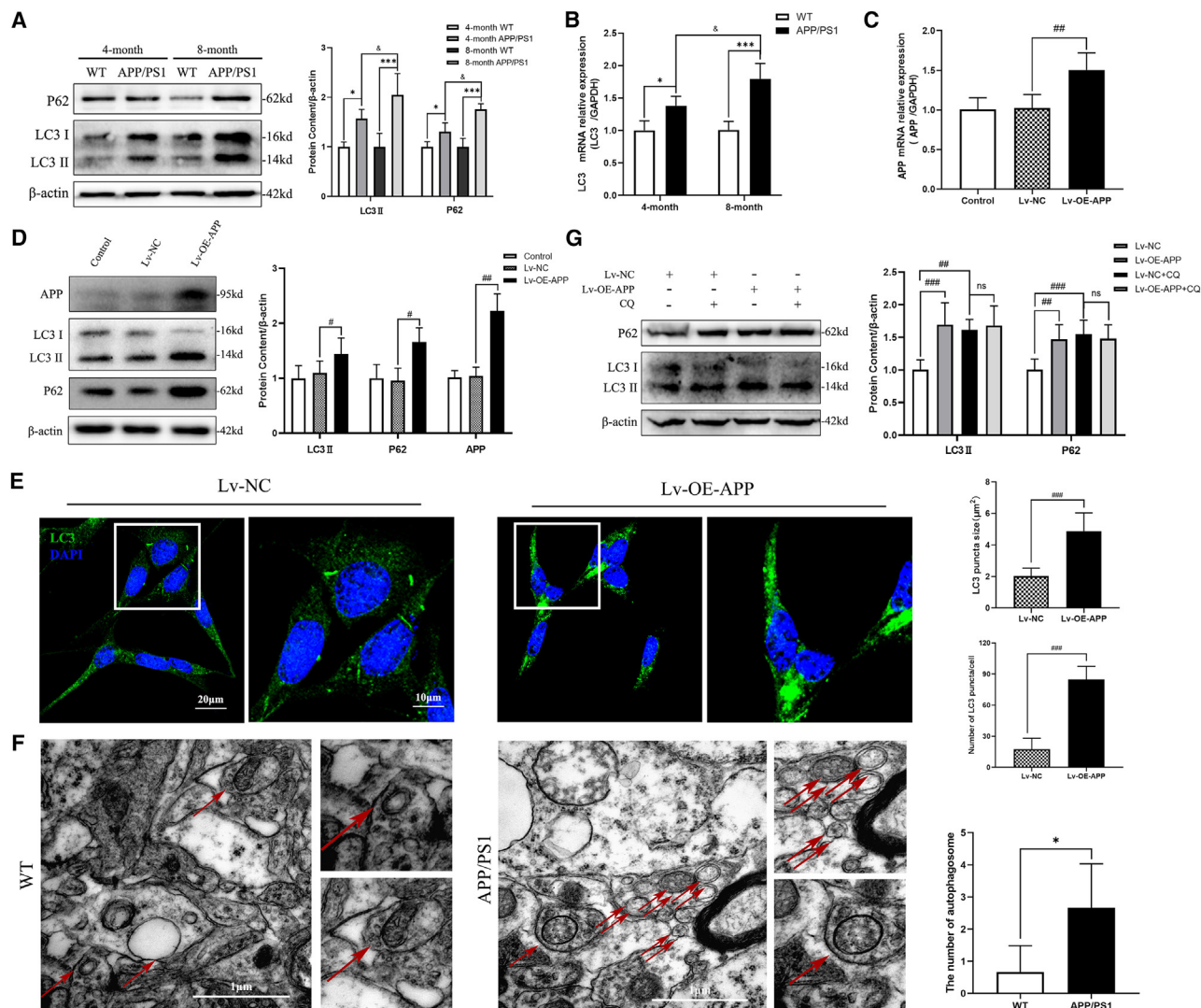
**Figure 1. Autophagosome-lysosome fusion is impaired in the AD model**

(A) LC3II and P62 protein expression levels in the hippocampal tissues of the 4-month-old/8-month-old WT and APP/PS1 groups.

(B) LC3 mRNA expression levels in the hippocampal tissues of the 4-month-old/8-month-old WT and APP/PS1 groups.

(C) RT-PCR verified the elevated levels of APP mRNA in HT22 cells.

(D) Western blot verified the elevated levels of APP protein in HT22 cells. The expression levels of the autophagy-related proteins LC3II and P62 were increased in APP-overexpressing HT22 cells.

(E) Fluorescence localization of LC3II in HT22 cells after APP overexpression; green indicates LC3 puncta, and blue indicates nuclei. Scale bar, 20 μm.

(F) Autophagosomes and autophagic lysosomes within neurons in the hippocampal tissues of 4-month-old WT mice and APP/PS1 mice. Red single arrows indicate autophagic lysosomes of a monolayer membrane; red double arrows indicate autophagic bodies of the bilayer membrane. Scale bar, 1 μm.

(G) Expression of LC3II and P62 in HT22 cells overexpressing APP after CQ interference. $n = 6$; ns, no significance; *$p < 0.05$ vs. the 4-month-old WT group; **$p < 0.01$ vs. the 4-month-old WT group; ***$p < 0.001$ vs. the 4-month-old WT group; $^{\&}p < 0.05$ vs. the 4-month APP/PS1 group; $^{\#}p < 0.05$ vs. the Lv-NC group; $^{\#\#}p < 0.01$ vs. the Lv-NC group; $^{\#\#\#}p < 0.001$ vs. the Lv-NC group. Data are represented as mean ± SD.

interfering RNA (siRNA)-mediated knockdown of STX17, LC3 mRNA expression increased, while LC3II and P62 protein expression also increased ($p < 0.05$) (Figures 3G and S1), which suggested that decreased expression of STX17 can further block autophagy. Additionally, the expression of LC3II and P62 decreased after STX17 overexpression ($p < 0.05$) (Figures 3H and S2); to a certain extent, STX17 reversed the autophagy blockade caused by AD. After chloroquine treatment, the

expression of LC3II and P62 tended to increase in the Lv-OE-APP+Lv-OE-STX17 group ($p < 0.05$), but there were no significant changes in the control group ($p > 0.05$) (Figure 3I). In addition, abnormal Aβ deposition increased after STX17 knockdown but decreased after STX17 overexpression (Figure 3J). These results suggested that STX17 promoted the fusion of autophagosomes and lysosomes, which in turn partially restored autophagic flux and cleared Aβ. In summary, our study demonstrated
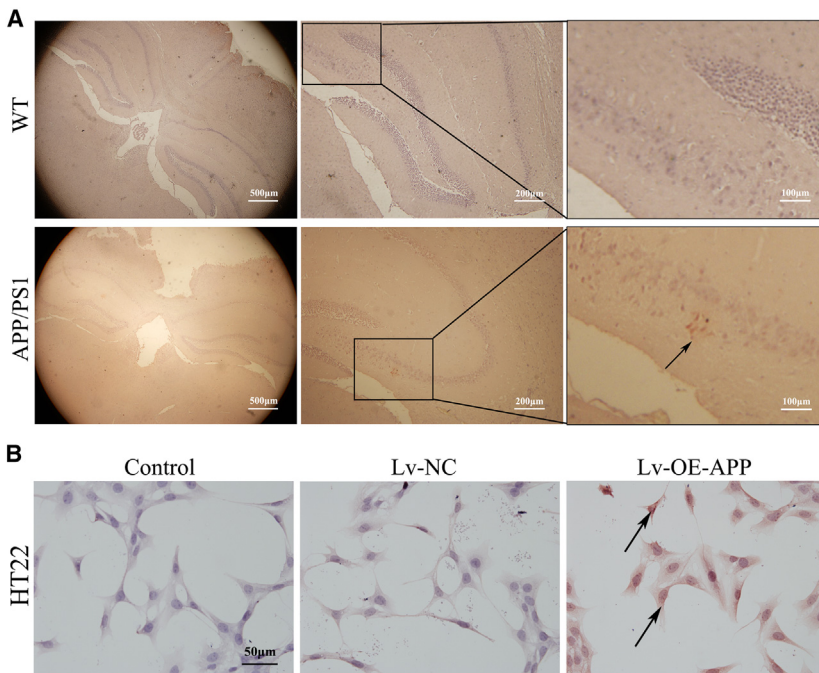
**Figure 2. Deposition of amyloid in hippocampal neurons in the AD model**
(A) Congo red staining of hippocampal tissues from the WT and APP/PS1 groups revealed amyloid deposition. Scale bars, 500 μm, 200 μm, and 100 μm.
(B) Intracellular Congo red staining of the control, Lv-NC, and Lv-OE-APP groups revealed amyloid deposition. $n = 3$; scale bar, 50 μm. The black arrows indicate amyloid-stained Congo red.

that STX17 contributes to autophagy activation and the fusion of autophagosomes and lysosomes, thereby promoting the clearance of Aβ.

### STX17 promotes autophagosome-lysosome fusion in hippocampal neurons via the SNARE complex

To further elucidate the function of STX17, the results showed that the binding of SNAP29 to STX17 in the Lv-OE-APP group was significantly lower than that in the Lv-NC group (Figure 4A). In addition, the binding of STX17 to SNAP29 in the Lv-OE-APP+Lv-OE-STX17 group increased after STX17 overexpression (Figure 4B). The colocalization of STX17 on autophagosomes and VAMP8 on lysosomes was observed by IF staining. Furthermore, the colocalization of STX17 and VAMP8 decreased after APP was overexpressed; on this basis, knocking down STX17 reduced the colocalization of STX17 and VAMP8 (Figure 4C). These results suggested that STX17 is a key factor in recruiting SNAP29 and VAMP8 to form SNARE complexes.

### The AD model showed circadian rhythm disturbance and decreased Bmal1 expression

To assess whether AD can entrain circadian rhythms of locomotor activity in the mouse, mice were housed in cages and subjected to a 12:12 Light-Dark (LD) schedule. After 10 days in baseline conditions, we started housing them in Dark-Dark (DD) schedule for 14 days. *In vitro*, we added Dexamethasone to synchronize cell cycle (Figure 5A). The activity time and amount of exercise of the mice were recorded by a wheel-running device. In the DD environment, the WT group had regular running-wheel activities and clear demarcations between movement and rest, and the activity phase was mainly concentrated on the subjective night. However, the APP/PS1 mice exhibited a significant in-

crease in fragmented arousal and activity during the day, and the results showed that the daytime activity of the APP/PS1 mice increased significantly compared with that of the WT mice ($p < 0.05$). The results showed that the free-running cycle of the WT group mice was $23.63 \pm 0.08$ h, and the free-running cycle of the APP/PS1 mice was $23.83 \pm 0.09$ h ($p < 0.05$) (Figure 5B). Additionally, APP/PS1 mice exhibit circadian rhythm disorders. The light on time of 8:00 during LD was set to CT0, and the expression of BMAL1 was detected by western blot at four time points, CT0, CT6, CT12, and CT18. The rhythm of BMAL1 expression was analyzed by JTK-CYCLE, and $p < 0.05$ was considered to indicate diurnal fluctuations in BMAL1 expression. The results revealed that the expression of BMAL1 protein in the WT group had obvious rhythmic fluctuations, and the expression of BMAL1 in hippocampal neurons decreased in the APP/PS1 group compared with that in the WT group (Figure 5C); in particular, BMAL1 expression decreased significantly at the CT0 and CT18 time points. On the other hand, the same trend of BMAL1 expression was also observed in HT22 cells after APP was overexpressed (Figure 5D). IF and plasmonuclear isolation also revealed that BMAL1 expression was reduced and that BMAL1 was concentrated mainly in the nucleus (Figures 5E and 5F).

### Bmal1 affects autophagy and Aβ deposition by regulating STX17 expression

The possible regulatory mechanism and binding site of BMAL1 were analyzed via the prediction website JASPAR, and the region was analyzed via JASPAR to identify possible transcription factor-binding sites (Figure 6A). We constructed a luciferase reporter of STX17. Overexpression of BMAL1 increased the luciferase activity of STX17, suggesting that BMAL1 can bind to the promoter of STX17 to promote transcription (Figure 6B). These results confirmed that BMAL1 could affect the transcription of STX17. After BMAL1 was overexpressed, autophagic flow and Aβ deposition were detected by western blotting and Congo red staining. BMAL1 and STX17 expression increased, and LC3II and P62 expression decreased after BMAL1 was overexpressed (Figure 6C), which partly indicated that overexpression of BMAL1 can restore autophagy flow. Furthermore, abnormal intracellular Aβ deposition was reduced after BMAL1 overexpression (Figure 6D). Taken together, these findings suggested that BMAL1 might clear intracellular Aβ via STX17.

## DISCUSSION

We found circadian rhythm disturbance, impaired autophagosome-lysosome fusion in hippocampal neurons, and decreased intracellular Aβ deposition in AD models. Through bioinformatics analysis, it was concluded that the decreased expression of STX17 was related to impaired autophagosome-lysosome fusion. We subsequently inhibited STX17 expression and found that STX17 may promote autophagosome-lysosome fusion through the formation of a complex of SNAP29 and VAMP8 to reduce Aβ deposition. In addition, motif analysis and luciferase assays suggested that the circadian rhythm protein BMAL1 can bind to the STX17 locus and affect autophagy. In summary, decreased expression of BMAL1 inhibited STX17 transcription and subsequently downregulated STX17 protein expression to reduce the formation of the STX17-SNAP29-VAMP8 complex, resulting in impaired autophagosome-lysosome fusion and abnormal accumulation of Aβ in the process of AD.

Increased expression of the LC3II and P62 proteins and blockade of autophagic flux occurred in a variety of AD models. At present, studies have shown that autophagy blockade may be caused by impaired fusion of autophagosomes and lysosomes. Consistently, our results indicated that abnormally deposited Aβ accumulated in AD models. The autophagy-lysosomal system plays an important role in the metabolism of Aβ, and autophagy promotes the degradation and clearance of APP and Aβ.[24,25] With increasing amounts of research, increasing evidence has shown that intracellular Aβ plays an important role in the AD process, and even more intracellular Aβ appears to precede extracellular Aβ.[26] The intracellular aggregation of Aβ disrupts the balance of intracellular and extracellular Aβ, resulting in a 10,000-fold increase in Aβ in the AD brain.[27] Therefore, intracellular Aβ accumulation is potentially correlated with early molecular changes prior to amyloid plaque formation. The enrichment of Aβ in late endosomes and lysosomes may be a key event leading to the molecular cascade of AD[28]; however, intracellular Aβ can also promote the intensification of Tau protein phosphorylation and the formation of toxic Tau oligomers.[29] Our study revealed that Aβ accumulated in the hippocampal tissue of 4-month-old APP/PS1 mice and APP-overexpressing HT22 cells. Other studies have also shown diffuse amyloid plaques in the cortex and hippocampus of 5-month-old APP/PS1 mice. If excess Aβ is produced in the brain and cannot be removed in time, it will accumulate to form amyloid plaques.[30] In addition, 6-month-old APP/PS1 double-transgenic mice not only exhibited Aβ deposition in the hippocampus and cortex but also exhibited neuronal damage.[31]

At present, autophagy is an important pathway for intracellular Aβ clearance, and autophagy degrades and recycles its own senescent or dysfunctional protein components to maintain cellular homeostasis and metabolic balance.[32] The fusion of autophagosomes and lysosomes is very important for maintaining the smooth circulation of autophagosomes. Disruption of the fusion of the two proteins obstructs autophagy flow, which affects the degradation of senescent proteins and abnormal protein aggregation in cells.[33] This study revealed that the expression of LC3II and P62 was increased in the AD model. Coincidentally, other studies have shown that LC3II and P62 expression is elevated in the hippocampus of 3-, 6-, and 10-month-old APP/PS1 mice.[34] Moreover, many studies have confirmed that autophagy and AD are closely related. Using the double-standard adenovirus GFP-RFP-LC3-labeled Aβ25-35, in which Aβ25-35 was found to increase the number of autophagosomes in SH-SY5Y cells and decrease the number of autophagic lysosomes, Aβ25-35 was shown to significantly hinder the fusion of autophagosomes and autolysosomes in SH-SY5Y cells.[35] This study also revealed that a large number of autophagic bodies accumulate in neurons in the hippocampal tissues of APP/PS1 double-transgenic mice. Recently, increasing evidence has shown that impairment of the autophagy-lysosomal pathway is associated with the pathogenesis of AD. Because autophagy blockade is caused by impaired autophagosome-lysosome fusion *in vitro*, this study showed that the protein expression of LC3II and P62 did not significantly change in APP-overexpressing HT22 cells after the addition of chloroquine by blocking the autophagosome-lysosome fusion process. In the case of autophagy progression, CQ can significantly increase the protein levels of LC3-II/LC3-I and P62, and, when autophagy is blocked, the protein expression of LC3II and P62 does not change significantly after CQ is added.[36] These findings confirmed the disorder of autophagosome-lysosome fusion in AD models. The autophagy-lysosomal pathway is damaged during the AD process, resulting in the obstruction of autophagic flow.

In this study, bioinformatics analysis revealed that STX17 is a differentially expressed SNARE protein in the brains of AD patients, which is associated with autophagosome-lysosome fusion, and that STX17 mRNA and protein expression are reduced in AD animal and cell models. Autophagy flow changed after STX17 intervention. Co-IP and IF colocalization revealed that STX17 may regulate the fusion of autophagosomes and lysosomes by binding to SNAP29 and VAMP8 to form the SNARE complex, further

**Figure 3. Decreased STX17 expression and abnormal Aβ deposition during AD**

(A) Significantly differentially expressed genes associated with autophagy in the brains of AD patients.

(B) GO enrichment of DEGs and KEGG pathway analysis.

(C) The GSEA analysis of autophagy.

(D and E) Changes in the expression of STX17 genes and proteins in the AD model.

(F) STX17 fluorescence in APP-overexpressing cells; green indicates STX17, and blue indicates the nucleus. Scale bar, 20 μm.

(G) Changes in LC3II and P62 expression after siRNA-mediated knockdown of STX17.

(H) Changes in LC3II and P62 expression after STX17 were overexpressed in APP-overexpressing HT22 cells.

(I) Expression of LC3II and P62 in HT22 cells overexpressing APP and STX17 after CQ interference.

(J) Interference with amyloid deposition after STX17 expression. $n = 6$; scale bar, 50 μm. $^*p < 0.05$ vs. the WT group; $^{**}p < 0.01$ vs. the WT group; $^#p < 0.05$ vs. the Lv-NC group; $^{##}p < 0.01$ vs. the Lv-NC group; $^{###}p < 0.001$ vs. the Lv-NC group; $^$p < 0.05$ vs. the Lv-OE-APP+Lv-NC group; $^{$$}p < 0.01$ vs. the Lv-OE-APP+Lv-NC group. Data are represented as mean ± SD.
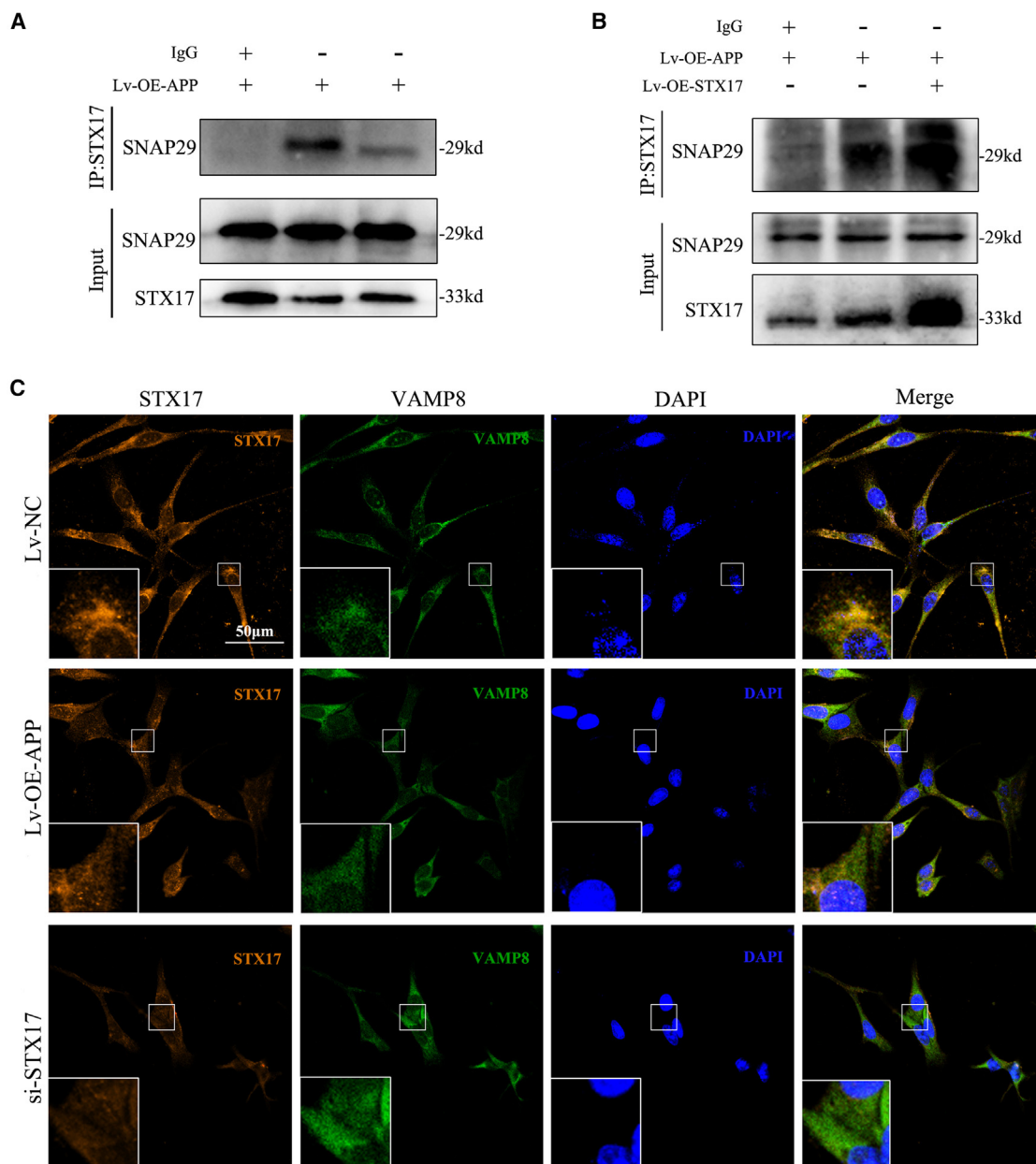
**Figure 4. The binding of STX17 to SNAP29 and VAMP8 is weakened during AD**

(A) After APP overexpression, STX17 and SNAP29 binding decreases; (B) after STX17 overexpression, APP overexpression increases the binding of STX17 to SNAP29 in cells; (C) STX17 is colocalized with VAMP8 by immunofluorescence; orange indicates STX17, green indicates VAMP8, and blue indicates the nucleus. $n = 3$; scale bar, 50 μm.

affecting the clearance of Aβ. Animals with STX17 mutations develop neuronal dysfunction and motor defects, suggesting that defects in autophagosome clearance may have an impact on various human diseases.[37] In mammalian cells, the parallelo-chelix bundle composed of autophagosome-localized Qa-SNARE STX17, Qbc-SNARE SNAP29, and lysosomal R-SNARE VAMP8 forms the SNARE complex, promoting autophagosome-lysosome fusion.[38,39] Among them, STX17 plays a major role in autophagy. On the one hand, since STX17 is a hairpin structure

formed by two transmembrane domains, each domain contains a glycine zipper[40]; on the other hand, STX17 is not present on unclosed autophagosomes but is recruited to autophagosome membranes immediately before or after autophagosome closure.[41] The subsequent recruitment of STX17 to intact autophagosomes can prevent the premature fusion of lysosomes with un-enclosed phagocytes, so the localization of STX17 to autophagosomes is particularly important for the formation of SNARE complexes. STX17 can promote the fusion of autophagosomes
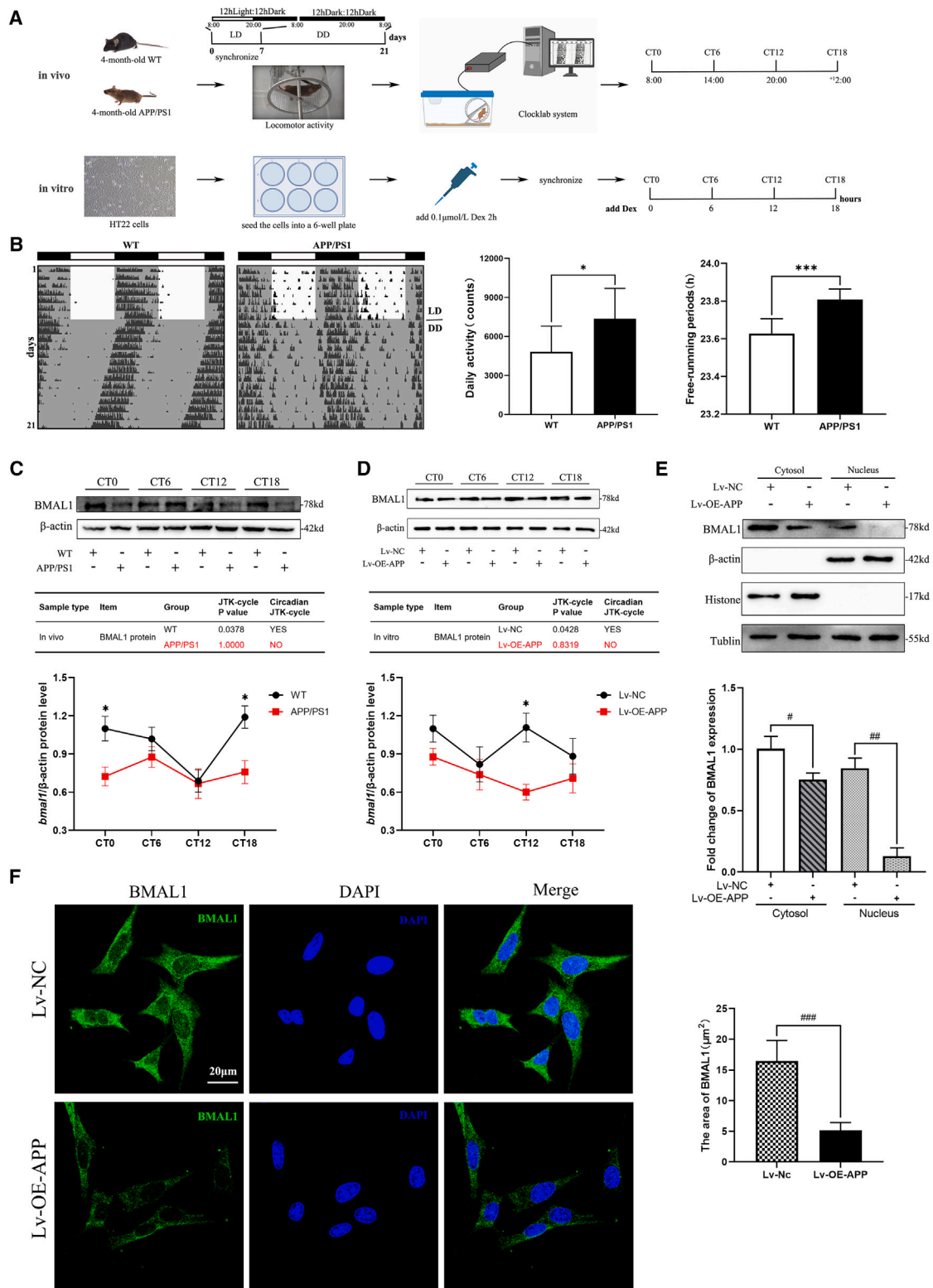
**Figure 5. The AD model showed circadian rhythm disturbance and decreased Bmal1 expression**

(A) The protocol of synchronize *in vivo* and *in vitro*.

(B) APP/PS1 mice displayed circadian rhythm disorders, increased daytime activity, and prolonged free-running cycles.

and lysosomes not only by forming SNARE complexes but also by recruiting HOPS complexes. RUB domain-containing protein-like (RUBCNL) can direct PtdIns3K and Homotypic Fusion and Protein Sorting Complex (HOPS) complexes to autophagosomes by interacting directly with STX17.[42] However, studies have shown that the binding of STX17 and HOPS during the fusion of autophagosomes and lysosomes does not appear to have an effect on STX17-SNAP29 interactions.[43,44] STX17 not only acts on the fusion process of autophagosomes and lysosomes but is also distributed in different subcells, including autophagosomes/autolysosomes, the endoplasmic reticulum (ER), the Golgi apparatus, the mitochondria-associated endoplasmic reticulum, and mitochondria, contributing to the regulatory function of STX17 in autophagy.[45,46] Our study revealed that decreased expression of STX17 reduced its binding to SNAP29. The deletion of STX17 can block the formation of the STX17-SNAP29-VAMP8 complex, and knocking out both STX16 and STX17 can completely block autophagic flux.[47] If impaired autophagosome-lysosomal fusion is induced by siRNA mutation or knockout of the STX17 gene, this approach is more specific than bafilomycin A1.[37] The use of siRNA to interfere with STX17 in human HeLa cells, HEK293 cells, and mouse fibroblasts cultured *in vitro* can induce autophagosome-lysosomal fusion disorders and significant accumulation of autophagosomes, which can be reversed by further cotransfection of anti-RNAi genes.[48] Many studies have shown that STX17 plays an important role in autophagy, especially in the fusion of autophagosomes and lysosomes, but the relationships among STX17, autophagy, and Aβ clearance are poorly understood.

Furthermore, by observing the wheel running of APP/PS1 mice, we found that APP/PS1 mice had rhythm disorders, suggesting that the occurrence of AD was closely related to circadian rhythm. Therefore, we determined that the expression of BMAL1 rhythm in the AD model was abnormal, and, through bioinformatics prediction, it was found that BMAL1 could be used as a transcription factor to regulate the transcription of STX17. Double luciferase reporter and chromatin coprecipitation assays also indicated that Bmal1 can bind to the STX17 promoter, thereby affecting STX17 transcription. A large number of studies have shown that there is a complex relationship between circadian rhythm disorders and AD pathology, and the early manifestations of the disease are reduced sleep efficiency, sleep fragmentation, and sleep-wake cycle disorders, even before the development of cognitive impairment.[49,50] Studies have shown that a lack of sleep due to circadian rhythm disturbances also increases the risk of AD, in which controlled sleep can affect AD-related pathologies in mouse models and that the sleep-wake cycle can regulate the level of pathogenic Aβ in the brain.[51,52] In this study, 4-month-old APP/PS1 double-transgenic mice were also found to exhibit sleep-wake cycle disturbance and Aβ deposition. Other experiments have confirmed that 3-month-old 3xTg-AD mice exhibit obvious circadian rhythm disorders, mainly due to

increased daytime activity and decreased nocturnal activity,[53] and 9-month-old APP/PS1 double-transgenic mice also exhibit circadian rhythm disturbances.[54]

The mammalian circadian clock basically relies on transcriptional activators (BMAL1 and CLOCK) to induce the transcription of inhibitors (Per and Cry), which causes the latter to accumulate over time until it reaches a level sufficient to inhibit its own activation.[55] This study revealed that the expression of the circadian clock gene Bmal1 decreased and that rhythm fluctuations were disrupted in AD animal and cell models. Studies using AD mouse models to explore the role of Aβ in regulating circadian rhythms and clock molecules have indicated that the circadian rhythm behavior of AD mice is altered and that the expression patterns of the circadian clock genes Bmal1 and Per2 are altered.[56] As an important core clock gene that regulates the expression of multiple genes, Bmal1 knockout alters the rhythm of Aβ interstitial fluid and intensifies Aβ plaque deposition in the hippocampus.[57] BMAL1 can act as a transcription factor to directly drive the transcription of downstream genes, such as the Reverse erythroblastosis virus (REV-ERB) protein involved in microglial activation, thereby regulating Aβ.[58] In recent years, the relationship between circadian rhythms and autophagy has gradually been revealed. Rhythmic changes in the volume and number of autophagic vesicles have been reported in cardiomyocytes, liver cells, kidneys, and pancreatic cells.[59] Recently, it has been shown that autophagy levels are controlled by several clock genes, notably Per2 and BMAL1.[60] For example, the BMAL1/CLOCK complex can induce the expression of ATG14, a gene related to the initiation of autophagy. BMAL1 induces autophagy through downregulation of mTORC1 signaling in cardiomyocytes, thereby protecting cardiomyocytes under hyperglycemic conditions.[61] Other studies revealed that the expression of LC3-I increased but the expression of P62 decreased, while Beclin-1 levels did not change in BMAL1$^{-/-}$ mouse muscle.[62] These findings indicate that circadian rhythm disorders can lead to autophagy dysfunction or decline. Bmal1, as an important element in the feedback loop of TTFLs, can bind to the E-box element on the clock gene to initiate the transcription of these genes.[63] In this study, a motif was used to predict the presence of binding sites between BMAL1 and STX17, and a dual-luciferase reporter assay revealed that BMAL1 can regulate STX17 transcription. Among them, STX17 is a clock control gene and can be regulated by clock genes such as Bmal1.[64] In addition, studies have shown that Bmal1 knockout can increase LC3 expression and p62 accumulation in cardiomyocytes, suggesting that Bmal1 is involved in the regulation of autophagosome-lysosome fusion.[65]

In summary, we found that the decrease in Bmal1 expression caused by circadian rhythm disturbance in APP/PS1 mice inhibited autophagosome-lysosome fusion and promoted

(C) Dysrhythmic expression of BMAL1 in the hippocampal nerve tissue of APP/PS1 mice.
(D) Dysrhythmic expression of BMAL1 in APP-overexpressing HT22 cells.
(E) Expression of BMAL1 in HT22 cell cytosol and nucleus after APP overexpression.
(F) Localization of BMAL1 in APP-overexpressing HT22 cells; green represents BMAL1, and blue represents the nucleus. $n$ = 6; scale bar, 20 μm.*$p$ < 0.05 vs. the WT group; ***$p$ < 0.001 vs. the WT group; #$p$ < 0.05 vs. the Lv-NC group; ##$p$ < 0.01 vs. the Lv-NC group; ###$p$ < 0.001 vs. the Lv-NC group. Data are represented as mean ± SD.
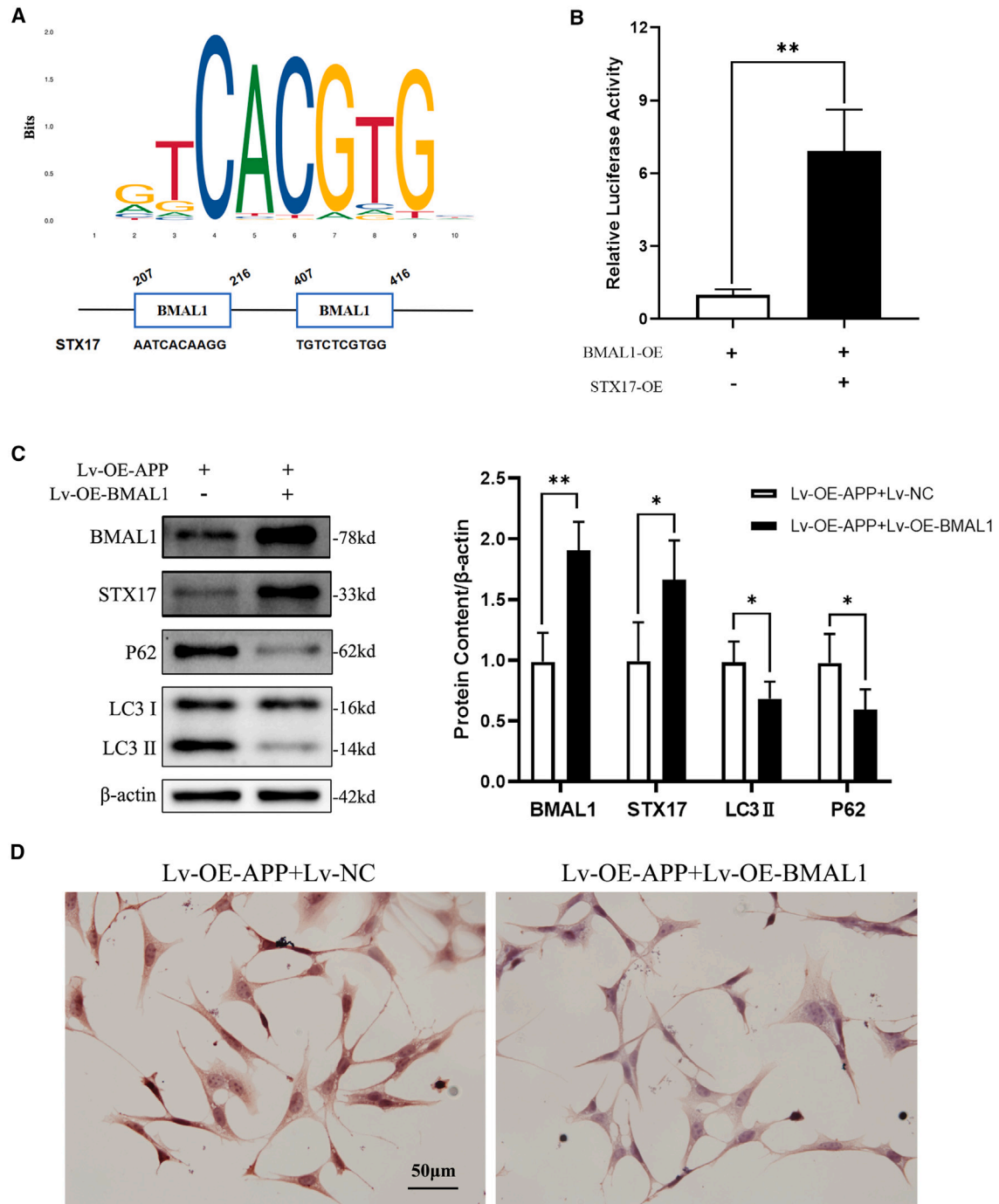
**Figure 6. BMAL1 regulates STX17 to affect autophagy and amyloid deposition**

(A) JASPAR analysis revealed the recognition sites of BMAL1 on the promoter sequence of STX17.

(B) Detection of luciferase activity after the STX17 promoter sequence plasmid and BMAL1 plasmid were transfected into HT22 cells.

(C) Autophagic flow was partially restored in APP-overexpressed HT22 after BMAL1 overexpression.

(D) Amyloid deposition decreases after BMAL1 overexpression. $n = 6$; scale bar, 50 μm. *$p < 0.05$ vs. the Lv-OE-APP+Lv-NC group; **$p < 0.01$ vs. the Lv-OE-APP+Lv-NC group. Data are represented as mean ± SD.

abnormal Aβ deposition. BMAL1 may influence autophagy through transcriptional regulation of STX17.

## Limitations of the study

This study has several limitations. First, the findings in APP/PS1 mice may not fully translate to human AD, necessitating further *in vivo* studies. Second, the focus on the BMAL1-STX17 pathway leaves other regulatory mechanisms in autophagy unexplored. Finally, the impact of circadian rhythm disturbances on other physiological or behavioral outcomes remains unaddressed, limiting the generalizability of the results.

## RESOURCE AVAILABILITY

### Lead contact

Further information and requests for resources and reagents should be directed to and will be fulfilled by the lead contact, Xiaohui Wang (163.wangxh@163.com).

### Materials availability

This study did not generate new unique reagents.

### Data and code availability

- Data: Original western blot images are publicly available as of the date of publication. Microscopy data reported in this paper will be shared by the lead contact upon request.
- Code: GEO (https://www.ncbi.nlm.nih.gov/gds/) was used for bioinformatics analysis to predict the genes associated with autophagy that are differentially expressed between normal controls and patients with AD. Gene expression data (GEO: GSE21779 published on Apr 01, 2011, and update on Mar 25, 2019) have been deposited at GEO and are publicly available as of the date of publication. According to the prediction results for different genes, GO terms and KEGG pathways were used to analyze all features. Heatmap was plotted by https://www.bioinformatics.com.cn, an online platform for data analysis and visualization. JASPAR analysis (http://jaspar.genereg.net/) revealed the binding sites.
- Additional information: Additional information and requests for resources and reagents used in this study should be directed to and will be fulfilled by the lead contact, Xiaohui Wang (163.wangxh@163.com).

## AUTHOR CONTRIBUTIONS

X.W. and L.W. designed the experiments. X.Z. performed the majority of the experiments and wrote the paper. T.M. and N.W. analyzed the data. L.Z. and Y.T. performed the confocal microscopy assays. K.D. and T.L. performed the coIP. X.W. and L.W. helped to revise the paper.

## DECLARATION OF INTERESTS

The authors declare no competing interests.

## STAR★METHODS

Detailed methods are provided in the online version of this paper and include the following:

- KEY RESOURCES TABLE
- EXPERIMENTAL MODEL AND STUDY PARTICIPANT DETAILS
  - Mice
- METHOD DETAILS
  - Transmission electron microscopy (TEM)
  - Congo red staining
  - Cell culture and reagents
  - siRNA transfections
  - RNA isolation and quantitative real-time PCR (qRT–PCR)
  - Western blot and antibodies
  - Immunoprecipitation (Co-IP)
  - Immunofluorescence staining
  - Locomotor activity measurement
  - Luciferase reporter assay
- QUANTIFICATION AND STATISTICAL ANALYSIS

## SUPPLEMENTAL INFORMATION

Supplemental information can be found online at https://doi.org/10.1016/j.isci.2024.111413.

## REFERENCES

1. Wightman, D.P., Jansen, I.E., Savage, J.E., Shadrin, A.A., Bahrami, S., Holland, D., Rongve, A., Børte, S., Winsvold, B.S., Drange, O.K., et al. (2021). A genome-wide association study with 1,126,563 individuals identifies new risk loci for Alzheimer's disease. Nat. Genet. *53*, 1276–1282. https://doi.org/10.1038/s41588-021-00921-z.

2. Plotkin, S.S., and Cashman, N.R. (2020). Passive immunotherapies targeting Abeta and tau in Alzheimer's disease. Neurobiol. Dis. *144*, 105010. https://doi.org/10.1016/j.nbd.2020.105010.

3. Zhou, J., Singh, N., Galske, J., Hudobenko, J., Hu, X., and Yan, R. (2023). BACE1 regulates expression of Clusterin in astrocytes for enhancing clearance of beta-amyloid peptides. Mol. Neurodegener. *18*, 31. https://doi.org/10.1186/s13024-023-00611-w.

4. Sun, Y., Liu, Z., Pi, Z., Song, F., Wu, J., and Liu, S. (2021). Poria cocos could ameliorate cognitive dysfunction in APP/PS1 mice by restoring imbalance of Abeta production and clearance and gut microbiota dysbiosis. Phytother Res. *35*, 2678–2690. https://doi.org/10.1002/ptr.7014.

5. Zhao, Y., Long, Z., Ding, Y., Jiang, T., Liu, J., Li, Y., Liu, Y., Peng, X., Wang, K., Feng, M., and He, G. (2020). Dihydroartemisinin Ameliorates Learning and Memory in Alzheimer's Disease Through Promoting Autophagosome-Lysosome Fusion and Autolysosomal Degradation for Abeta Clearance. Front. Aging Neurosci. *12*, 47. https://doi.org/10.3389/fnagi.2020.00047.

6. Israel, M.A., Yuan, S.H., Bardy, C., Reyna, S.M., Mu, Y., Herrera, C., Hefferan, M.P., Van Gorp, S., Nazor, K.L., Boscolo, F.S., et al. (2012). Probing sporadic and familial Alzheimer's disease using induced pluripotent stem cells. Nature *482*, 216–220. https://doi.org/10.1038/nature10821.

7. Li, Y., Zhang, J., Wan, J., Liu, A., and Sun, J. (2020). Melatonin regulates Abeta production/clearance balance and Abeta neurotoxicity: A potential therapeutic molecule for Alzheimer's disease. Biomed. Pharmacother. *132*, 110887. https://doi.org/10.1016/j.biopha.2020.110887.

8. Zhang, W., Xu, C., Sun, J., Shen, H.M., Wang, J., and Yang, C. (2022). Impairment of the autophagy-lysosomal pathway in Alzheimer's diseases:

Pathogenic mechanisms and therapeutic potential. Acta Pharm. Sin. B *12*, 1019–1040. https://doi.org/10.1016/j.apsb.2022.01.008.

9. Shen, Q., Shi, Y., Liu, J., Su, H., Huang, J., Zhang, Y., Peng, C., Zhou, T., Sun, Q., Wan, W., and Liu, W. (2021). Acetylation of STX17 (syntaxin 17) controls autophagosome maturation. Autophagy *17*, 1157–1169. https://doi.org/10.1080/15548627.2020.1752471.

10. Saleeb, R.S., Kavanagh, D.M., Dun, A.R., Dalgarno, P.A., and Duncan, R.R. (2019). A VPS33A-binding motif on syntaxin 17 controls autophagy completion in mammalian cells. J. Biol. Chem. *294*, 4188–4201. https://doi.org/10.1074/jbc.RA118.005947.

11. Zhu, Y., Wang, X., Hu, M., Yang, T., Xu, H., Kang, X., Chen, X., Jiang, L., Gao, R., and Wang, J. (2022). Targeting Abeta and p-Tau Clearance in Methamphetamine-Induced Alzheimer's Disease-Like Pathology: Roles of Syntaxin 17 in Autophagic Degradation in Primary Hippocampal Neurons. Oxid. Med. Cell. Longev. *2022*, 3344569. https://doi.org/10.1155/2022/3344569.

12. Zhang, L., Fang, Y., Zhao, X., Zheng, Y., Ma, Y., Li, S., Huang, Z., and Li, L. (2021). BRUCE silencing leads to axonal dystrophy by repressing autophagosome-lysosome fusion in Alzheimer's disease. Transl. Psychiatry *11*, 421. https://doi.org/10.1038/s41398-021-01427-2.

13. Wang, C., and Holtzman, D.M. (2020). Bidirectional relationship between sleep and Alzheimer's disease: role of amyloid, tau, and other factors. Neuropsychopharmacology *45*, 104–120. https://doi.org/10.1038/s41386-019-0478-5.

14. van Someren, E.J., Hagebeuk, E.E., Lijzenga, C., Scheltens, P., de Rooij, S.E., Jonker, C., Pot, A.M., Mirmiran, M., and Swaab, D.F. (1996). Circadian rest-activity rhythm disturbances in Alzheimer's disease. Biol. Psychiatry *40*, 259–270. https://doi.org/10.1016/0006-3223(95)00370-3.

15. Wu, H., Dunnett, S., Ho, Y.S., and Chang, R.C.C. (2019). The role of sleep deprivation and circadian rhythm disruption as risk factors of Alzheimer's disease. Front. Neuroendocrinol. *54*, 100764. https://doi.org/10.1016/j.yfrne.2019.100764.

16. Xiong, X., Hu, T., Yin, Z., Zhang, Y., Chen, F., and Lei, P. (2022). Research advances in the study of sleep disorders, circadian rhythm disturbances and Alzheimer's disease. Front. Aging Neurosci. *14*, 944283. https://doi.org/10.3389/fnagi.2022.944283.

17. Zhao, B., Liu, P., Wei, M., Li, Y., Liu, J., Ma, L., Shang, S., Jiang, Y., Huo, K., Wang, J., and Qu, Q. (2019). Chronic Sleep Restriction Induces Abeta Accumulation by Disrupting the Balance of Abeta Production and Clearance in Rats. Neurochem. Res. *44*, 859–873. https://doi.org/10.1007/s11064-019-02719-2.

18. Roh, J.H., Huang, Y., Bero, A.W., Kasten, T., Stewart, F.R., Bateman, R.J., and Holtzman, D.M. (2012). Disruption of the sleep-wake cycle and diurnal fluctuation of beta-amyloid in mice with Alzheimer's disease pathology. Sci. Transl. Med. *4*, 150ra122. https://doi.org/10.1126/scitranslmed.3004291.

19. Steen, E., Terry, B.M., Rivera, E.J., Cannon, J.L., Neely, T.R., Tavares, R., Xu, X.J., Wands, J.R., and de la Monte, S.M. (2005). Impaired insulin and insulin-like growth factor expression and signaling mechanisms in Alzheimer's disease–is this type 3 diabetes? J. Alzheimers Dis. *7*, 63–80. https://doi.org/10.3233/jad-2005-7107.

20. Bellanti, F., Iannelli, G., Blonda, M., Tamborra, R., Villani, R., Romano, A., Calcagnini, S., Mazzoccoli, G., Vinciguerra, M., Gaetani, S., et al. (2017). Alterations of Clock Gene RNA Expression in Brain Regions of a Triple Transgenic Model of Alzheimer's Disease. J. Alzheimers Dis. *59*, 615–631. https://doi.org/10.3233/JAD-160942.

21. Holland, W.L., Adams, A.C., Brozinick, J.T., Bui, H.H., Miyauchi, Y., Kusminski, C.M., Bauer, S.M., Wade, M., Singhal, E., Cheng, C.C., et al. (2013). An FGF21-adiponectin-ceramide axis controls energy expenditure and insulin action in mice. Cell Metab. *17*, 790–797. https://doi.org/10.1016/j.cmet.2013.03.019.

22. Wang, L., Zhao, J., Wang, C.T., Hou, X.H., Ning, N., Sun, C., Guo, S., Yuan, Y., Li, L., Hölscher, C., and Wang, X.H. (2020). D-Ser2-oxyntomodulin ameliorated Abeta31-35-induced circadian rhythm disorder in mice. CNS Neurosci. Ther. *26*, 343–354. https://doi.org/10.1111/cns.13211.

23. Perelis, M., Marcheva, B., Ramsey, K.M., Schipma, M.J., Hutchison, A.L., Taguchi, A., Peek, C.B., Hong, H., Huang, W., Omura, C., et al. (2015). Pancreatic beta cell enhancers regulate rhythmic transcription of genes controlling insulin secretion. Science *350*, aac4250. https://doi.org/10.1126/science.aac4250.

24. Zhou, F., van Laar, T., Huang, H., and Zhang, L. (2011). APP and APLP1 are degraded through autophagy in response to proteasome inhibition in neuronal cells. Protein Cell *2*, 377–383. https://doi.org/10.1007/s13238-011-1047-9.

25. Rahman, M.A., Rahman, M.S., Rahman, M.D.H., Rasheduzzaman, M., Mamun-Or-Rashid, A., Uddin, M.J., Rahman, M.R., Hwang, H., Pang, M.G., and Rhim, H. (2020). Modulatory Effects of Autophagy on APP Processing as a Potential Treatment Target for Alzheimer's Disease. Biomedicines *9*, 5. https://doi.org/10.3390/biomedicines9010005.

26. Habif, M., Do Carmo, S., Báez, M.V., Colettis, N.C., Cercato, M.C., Salas, D.A., Acutain, M.F., Sister, C.L., Berkowicz, V.L., Canal, M.P., et al. (2020). Early Long-Term Memory Impairment and Changes in the Expression of Synaptic Plasticity-Associated Genes, in the McGill-R-Thy1-APP Rat Model of Alzheimer's-Like Brain Amyloidosis. Front. Aging Neurosci. *12*, 585873. https://doi.org/10.3389/fnagi.2020.585873.

27. Roos, T.T., Garcia, M.G., Martinsson, I., Mabrouk, R., Israelsson, B., Deierborg, T., Kobro-Flatmoen, A., Tanila, H., and Gouras, G.K. (2021). Neuronal spreading and plaque induction of intracellular Abeta and its disruption of Abeta homeostasis. Acta Neuropathol. *142*, 669–687. https://doi.org/10.1007/s00401-021-02345-9.

28. Maesako, M., Houser, M.C.Q., Turchyna, Y., Wolfe, M.S., and Berezovska, O. (2022). Presenilin/gamma-Secretase Activity Is Located in Acidic Compartments of Live Neurons. J. Neurosci. *42*, 145–154. https://doi.org/10.1523/JNEUROSCI.1698-21.2021.

29. Zhang, H., Wei, W., Zhao, M., Ma, L., Jiang, X., Pei, H., Cao, Y., and Li, H. (2021). Interaction between Abeta and Tau in the Pathogenesis of Alzheimer's Disease. Int. J. Biol. Sci. *17*, 2181–2192. https://doi.org/10.7150/ijbs.57078.

30. Lin, S.Y., Ma, J., An, J.X., Qian, X.Y., Wang, Y., Cope, D.K., and Williams, J.P. (2019). Ozone Inhibits APP/Abeta Production and Improves Cognition in an APP/PS1 Transgenic Mouse Model. Neuroscience *418*, 110–121. https://doi.org/10.1016/j.neuroscience.2019.07.027.

31. Zhang, H., Su, Y., Sun, Z., Chen, M., Han, Y., Li, Y., Dong, X., Ding, S., Fang, Z., Li, W., and Li, W. (2021). Ginsenoside Rg1 alleviates Abeta deposition by inhibiting NADPH oxidase 2 activation in APP/PS1 mice. J. Ginseng Res. *45*, 665–675. https://doi.org/10.1016/j.jgr.2021.03.003.

32. Levine, B., and Kroemer, G. (2008). Autophagy in the pathogenesis of disease. Cell *132*, 27–42. https://doi.org/10.1016/j.cell.2007.12.018.

33. Zhou, J., Tan, S.H., Nicolas, V., Bauvy, C., Yang, N.D., Zhang, J., Xue, Y., Codogno, P., and Shen, H.M. (2013). Activation of lysosomal function in the course of autophagy via mTORC1 suppression and autophagosome-lysosome fusion. Cell Res. *23*, 508–523. https://doi.org/10.1038/cr.2013.11.

34. Long, Z., Chen, J., Zhao, Y., Zhou, W., Yao, Q., Wang, Y., and He, G. (2020). Dynamic changes of autophagic flux induced by Abeta in the brain of postmortem Alzheimer's disease patients, animal models and cell models. Aging (Albany NY) *12*, 10912–10930. https://doi.org/10.18632/aging.103305.

35. Ji, Y., Hu, Y., Ren, J., Khanna, R., Yao, Y., Chen, Y., Li, Q., and Sun, L. (2019). CRMP2-derived peptide ST2-104 (R9-CBD3) protects SH-SY5Y neuroblastoma cells against Abeta(25-35)-induced neurotoxicity by inhibiting the pCRMP2/NMDAR2B signaling pathway. Chem. Biol. Interact. *305*, 28–39. https://doi.org/10.1016/j.cbi.2019.03.005.

36. Bi, D., Yao, L., Lin, Z., Chi, L., Li, H., Xu, H., Du, X., Liu, Q., Hu, Z., Lu, J., and Xu, X. (2021). Unsaturated mannuronate oligosaccharide ameliorates beta-amyloid pathology through autophagy in Alzheimer's disease cell

models. Carbohydr. Polym. *251*, 117124. https://doi.org/10.1016/j.carbpol.2020.117124.

37. Tampellini, D., Rahman, N., Lin, M.T., Capetillo-Zarate, E., and Gouras, G.K. (2011). Impaired beta-amyloid secretion in Alzheimer's disease pathogenesis. J. Neurosci. *31*, 15384–15390. https://doi.org/10.1523/JNEUROSCI.2986-11.2011.

38. Kim, D.K., Jeong, H., Bae, J., Cha, M.Y., Kang, M., Shin, D., Ha, S., Hyeon, S.J., Kim, H., Suh, K., et al. (2022). Abeta-induced mitochondrial dysfunction in neural progenitors controls KDM5A to influence neuronal differentiation. Exp. Mol. Med. *54*, 1461–1471. https://doi.org/10.1038/s12276-022-00841-w.

39. Itakura, E., Kishi-Itakura, C., and Mizushima, N. (2012). The hairpin-type tail-anchored SNARE syntaxin 17 targets to autophagosomes for fusion with endosomes/lysosomes. Cell *151*, 1256–1269. https://doi.org/10.1016/j.cell.2012.11.001.

40. Ashrafi, G., Schlehe, J.S., LaVoie, M.J., and Schwarz, T.L. (2014). Mitophagy of damaged mitochondria occurs locally in distal neuronal axons and requires PINK1 and Parkin. J. Cell Biol. *206*, 655–670. https://doi.org/10.1083/jcb.201401070.

41. Cheng, X.T., Zhou, B., Lin, M.Y., Cai, Q., and Sheng, Z.H. (2015). Axonal autophagosomes recruit dynein for retrograde transport through fusion with late endosomes. J. Cell Biol. *209*, 377–386. https://doi.org/10.1083/jcb.201412046.

42. Cheng, X., Ma, X., Ding, X., Li, L., Jiang, X., Shen, Z., Chen, S., Liu, W., Gong, W., and Sun, Q. (2017). Pacer Mediates the Function of Class III PI3K and HOPS Complexes in Autophagosome Maturation by Engaging Stx17. Mol. Cell *65*, 1029–1043.e5. https://doi.org/10.1016/j.molcel.2017.02.010.

43. Lustbader, J.W., Cirilli, M., Lin, C., Xu, H.W., Takuma, K., Wang, N., Caspersen, C., Chen, X., Pollak, S., Chaney, M., et al. (2004). ABAD directly links Abeta to mitochondrial toxicity in Alzheimer's disease. Science *304*, 448–452. https://doi.org/10.1126/science.1091230.

44. Cummings, J.L., Goldman, D.P., Simmons-Stern, N.R., and Ponton, E. (2022). The costs of developing treatments for Alzheimer's disease: A retrospective exploration. Alzheimers Dement. *18*, 469–477. https://doi.org/10.1002/alz.12450.

45. Rong, Y., Zhang, S., Nandi, N., Wu, Z., Li, L., Liu, Y., Wei, Y., Zhao, Y., Yuan, W., Zhou, C., et al. (2022). STING controls energy stress-induced autophagy and energy metabolism via STX17. J. Cell Biol. *221*, e202202060. https://doi.org/10.1083/jcb.202202060.

46. Tanaka, Y., and Chen, Z.J. (2012). STING specifies IRF3 phosphorylation by TBK1 in the cytosolic DNA signaling pathway. Sci. Signal. *5*, ra20. https://doi.org/10.1126/scisignal.2002521.

47. Long, J.M., and Holtzman, D.M. (2019). Alzheimer Disease: An Update on Pathobiology and Treatment Strategies. Cell *179*, 312–339. https://doi.org/10.1016/j.cell.2019.09.001.

48. Knight, R., Khondoker, M., Magill, N., Stewart, R., and Landau, S. (2018). A Systematic Review and Meta-Analysis of the Effectiveness of Acetylcholinesterase Inhibitors and Memantine in Treating the Cognitive Symptoms of Dementia. Dement. Geriatr. Cogn. Disord *45*, 131–151. https://doi.org/10.1159/000486546.

49. Sharma, A., Sethi, G., Tambuwala, M.M., Aljabali, A.A.A., Chellappan, D.K., Dua, K., and Goyal, R. (2021). Circadian Rhythm Disruption and Alzheimer's Disease: The Dynamics of a Vicious Cycle. Curr. Neuropharmacol. *19*, 248–264. https://doi.org/10.2174/1570159X18666200429013041.

50. LeVault, K.R., Tischkau, S.A., and Brewer, G.J. (2016). Circadian Disruption Reveals a Correlation of an Oxidative GSH/GSSG Redox Shift with Learning and Impaired Memory in an Alzheimer's Disease Mouse Model. J. Alzheimers Dis. *49*, 301–316. https://doi.org/10.3233/JAD-150026.

51. Musiek, E.S., Xiong, D.D., and Holtzman, D.M. (2015). Sleep, circadian rhythms, and the pathogenesis of Alzheimer disease. Exp. Mol. Med. *47*, e148. https://doi.org/10.1038/emm.2014.121.

52. Shokri-Kojori, E., Wang, G.J., Wiers, C.E., Demiral, S.B., Guo, M., Kim, S.W., Lindgren, E., Ramirez, V., Zehra, A., Freeman, C., et al. (2018). beta-Amyloid accumulation in the human brain after one night of sleep deprivation. Proc. Natl. Acad. Sci. USA *115*, 4483–4488. https://doi.org/10.1073/pnas.1721694115.

53. Sterniczuk, R., Antle, M.C., Laferla, F.M., and Dyck, R.H. (2010). Characterization of the 3xTg-AD mouse model of Alzheimer's disease: part 2. Behavioral and cognitive changes. Brain Res. *1348*, 149–155. https://doi.org/10.1016/j.brainres.2010.06.011.

54. Zhou, F., Yan, X.D., Wang, C., He, Y.X., Li, Y.Y., Zhang, J., Wang, Z.J., Cai, H.Y., Qi, J.S., and Wu, M.N. (2020). Suvorexant ameliorates cognitive impairments and pathology in APP/PS1 transgenic mice. Neurobiol. Aging *91*, 66–75. https://doi.org/10.1016/j.neurobiolaging.2020.02.020.

55. Reddy, A.B., and Rey, G. (2014). Metabolic and nontranscriptional circadian clocks: eukaryotes. Annu. Rev. Biochem. *83*, 165–189. https://doi.org/10.1146/annurev-biochem-060713-035623.

56. Song, H., Moon, M., Choe, H.K., Han, D.H., Jang, C., Kim, A., Cho, S., Kim, K., and Mook-Jung, I. (2015). Abeta-induced degradation of BMAL1 and CBP leads to circadian rhythm disruption in Alzheimer's disease. Mol. Neurodegener. *10*, 13. https://doi.org/10.1186/s13024-015-0007-x.

57. McKee, C.A., Lee, J., Cai, Y., Saito, T., Saido, T., and Musiek, E.S. (2022). Astrocytes deficient in circadian clock gene Bmal1 show enhanced activation responses to amyloid-beta pathology without changing plaque burden. Sci. Rep. *12*, 1796. https://doi.org/10.1038/s41598-022-05862-z.

58. Lee, J., Kim, D.E., Griffin, P., Sheehan, P.W., Kim, D.H., Musiek, E.S., and Yoon, S.Y. (2020). Inhibition of REV-ERBs stimulates microglial amyloid-beta clearance and reduces amyloid plaque deposition in the 5XFAD mouse model of Alzheimer's disease. Aging Cell *19*, e13078. https://doi.org/10.1111/acel.13078.

59. Gao, D., Ma, T., Gao, L., Zhang, J., Zhang, H., Zhang, L., Dong, H., Li, Y., Zhao, L., Liu, W., et al. (2023). Autophagy activation attenuates the circadian clock oscillators in U2OS cells via the ATG5 pathway. Cell. Signal. *101*, 110502. https://doi.org/10.1016/j.cellsig.2022.110502.

60. Zhang, T.W., Li, Z.F., Dong, J., and Jiang, L.B. (2020). The circadian rhythm in intervertebral disc degeneration: an autophagy connection. Exp. Mol. Med. *52*, 31–40. https://doi.org/10.1038/s12276-019-0372-6.

61. Qiao, L., Guo, B., Zhang, H., Yang, R., Chang, L., Wang, Y., Jin, X., Liu, S., and Li, Y. (2017). The clock gene, brain and muscle Arnt-like 1, regulates autophagy in high glucose-induced cardiomyocyte injury. Oncotarget *8*, 80612–80624. https://doi.org/10.18632/oncotarget.20811.

62. Scotton, C., Bovolenta, M., Schwartz, E., Falzarano, M.S., Martoni, E., Passarelli, C., Armaroli, A., Osman, H., Rodolico, C., Messina, S., et al. (2016). Deep RNA profiling identified CLOCK and molecular clock genes as pathophysiological signatures in collagen VI myopathy. J. Cell Sci. *129*, 1671–1684. https://doi.org/10.1242/jcs.175927.

63. Hastings, M.H., Maywood, E.S., and O'Neill, J.S. (2008). Cellular circadian pacemaking and the role of cytosolic rhythms. Curr. Biol. *18*, R805–R815. https://doi.org/10.1016/j.cub.2008.07.021.

64. Zhang, W., Xiong, Y., Tao, R., Panayi, A.C., Mi, B., and Liu, G. (2022). Emerging Insight Into the Role of Circadian Clock Gene BMAL1 in Cellular Senescence. Front. Endocrinol. *13*, 915139. https://doi.org/10.3389/fendo.2022.915139.

65. McGinnis, G.R., Tang, Y., Brewer, R.A., Brahma, M.K., Stanley, H.L., Shanmugam, G., Rajasekaran, N.S., Rowe, G.C., Frank, S.J., Wende, A.R., et al. (2017). Genetic disruption of the cardiomyocyte circadian clock differentially influences insulin-mediated processes in the heart. J. Mol. Cell. Cardiol. *110*, 80–95. https://doi.org/10.1016/j.yjmcc.2017.07.005.

## STAR★METHODS

### KEY RESOURCES TABLE

| REAGENT or RESOURCE | SOURCE | IDENTIFIER |
|---|---|---|
| **Antibodies** | | |
| Anti-LC3B antibody | Abcam | Cat #ab192890 |
| BMAL1 (D2L7G) Rabbit mAb | Cell Signaling Technology | Cat #14020S |
| STX17 Polyclonal antibody | Proteintech | Cat #17815-1-AP |
| VAMP8 Polyclonal antibody | Proteintech | Cat #15546-1-AP |
| SNAP29 Polyclonal antibody | Proteintech | Cat #12704-1-AP |
| Anti-SQSTM1 / p62 antibody | Abcam | Cat #ab109012 |
| Anti-Amyloid Precursor Protein antibody | Abcam | Cat #ab32136 |
| **Bacterial and virus strains** | | |
| Lentivirus-overexpressing STX17 | Shanghai Genechem | N/A |
| Lentivirus-overexpressing BMAL1 | Shanghai Genechem | N/A |
| STX17-siRNA | Hanbio Biotechnology | N/A |
| **Chemicals, peptides, and recombinant proteins** | | |
| RNAiso Plus | TaKaRa | Cat #9109 |
| RIPA buffer | Boster | Cat #AR0102 |
| Glutaraldehyde,2.5%(EM Grade) | Solarbio | Cat #P1126 |
| **Critical commercial assays** | | |
| PrimeScript RT Master Mix | TaKaRa | Cat #RR036A |
| SYBR Premix Ex TaqTMII | TaKaRa | Cat #DRR041A |
| **Experimental models: Cell lines** | | |
| HT22 | Chinese Academy of Sciences Cell Bank | CSTR:19375.09.3101MOUGNM47 |
| **Experimental models: Organisms/strains** | | |
| SPF mice | Model Animal Research Center | APP/PS1 transgenic mice |
| **Software and algorithms** | | |
| ImageJ | ImageJ | https://imagej.nih.gov/ij/ |
| GraphPad Prism | GraphPad Prism | https://www.graphpad.com/ |
| **Other** | | |
| Code of GSE21779 | GEO | https://www.ncbi.nlm.nih.gov/gds/ |
| Code for data analysis and visualization | bioinformatics | https://www.bioinformatics.com.cn |
| Code for revealed the binding sites | JASPAR | http://jaspar.genereg.net/ |
| Data: Western Blot and Microscopy data | Lead contact | 163.wangxh@163.com |

### EXPERIMENTAL MODEL AND STUDY PARTICIPANT DETAILS

#### Mice

APP/PS1 mice and WT mice, acquired from the Model Animal Research Center of Nanjing University, were bred on a C57BL/6 background and maintained under a 12-hour light/12-hour dark cycle until they reached 4 months (n=20, male) and 8 months(n=4, male), n refers to the number of animals. Subsequently, 4-month-old mice were placed in dark-dark conditions for 14 days to observe carcadian rhythm. The use of animals complied with the national and Shanxi Medical University experimental animal use regulations (SYXK2019-0008).

### METHOD DETAILS

#### Transmission electron microscopy (TEM)

The hippocampi of the mice were rinsed and fixed at 4°C for 1 hour in a solution of 2.5% glutaraldehyde supplemented with 0.1 M phosphate-buffered saline (PBS), followed by postfixation in 1.0% osmium tetroxide for 3 hours. Subsequently, the cells were

collected by scraping, centrifuged, gradually dehydrated in ethanol solutions, and embedded in Epon Araldite blocks. Ultrathin sections (60–80 nm) were prepared using an Ultracut Microtome (UC7; Leica), stained with 4% aqueous uranyl acetate and lead citrate for 5 minutes, and then examined using a transmission electron microscope (TEM) operating at 200 kV (Tecnai G2 20 Twin, FEI).

### Congo red staining

HT22 cells were fixed with 4% paraformaldehyde for 10 minutes, followed by thorough rinsing with distilled water. Subsequently, they were immersed in modified Highman stain for 5 minutes and then treated dropwise with Highman differentiation solution for a few seconds under microscopic observation and control conditions. After rinsing with tap water, the cells were lightly stained with Mayer's hematoxylin for 1 min, followed by another rinse with tap water. Finally, the sections were stepwise dehydrated with graded ethanol, rendered transparent with xylene, and sealed with neutral gum.

### Cell culture and reagents

HT22 cells were purchased from the Chinese Academy of Sciences Cell Bank. Prior to cell treatment, the stock solutions were diluted to concentrations ranging from 100 to 200 $\mu$M in serum-free medium (DMEM + 1% penicillin–streptomycin). Chloroquine (MCE) was dissolved in sterile water and stored in aliquots at $-20^\circ$C. Stocks were subsequently diluted to concentrations of 20 or 40 $\mu$M in serum-free medium before being administered to cells. To synchronize cell rhythms in assays, cells were treated with 0.1 $\mu$M dexamethasone for 2 hours.Cell passaging and plating: discard the original culture rack, wash with PBS three times, add trypsin containing 0.25% EDTA to digest the adherent HT22 cells, add complete medium to terminate the reaction after the cells become round, centrifuge (1000rpm, 5min), discard the supernatant, resuspend the cell pellet with complete medium, and perform cell passaging or plating at an appropriate density.

### siRNA transfections

STX17-siRNA was obtained from Hanbio Biotechnology (Shanghai, China). The sequences of both the STX17-targeting and control siRNAs used were as provided. These siRNA oligonucleotides were transfected into HT22 cells at a concentration of 100 nM using RNA-fit Hanbio Biotechnology (Shanghai, China) following the manufacturer's guidelines.

### RNA isolation and quantitative real-time PCR (qRT−PCR)

TRIzol extraction kits (Invitrogen, US) were used to extract total RNA according to the manufacturer's protocol. To prevent potential DNA contamination, the extracted total RNA was treated with RNase-free DNase I (TaKaRa, Japan) before being reverse transcribed by a set of custom sequence-specific primers and M-MLV reverse transcriptase. The total RNA used as the template for reverse transcription was approximately 1 $\mu$g, and the concentration of the cDNA used for qRT−PCR was 100 ng/$\mu$L. The primers used for amplification were as follows: GAPDH sense, 5'-AAATGGTGAAGGTCGGTGTGAAC-3' and antisense, 5'-CAACAATCTCCACTTTGCCACTG-3'; APP sense, 5'-GCAATGATCTCCCGCTGGTA-3' and antisense, 5'-AACTTTGGGTTGACACGCTG-3'; and LC3II sense, 5'-GCGCTTGCAGCTCAATGCTA-3' and antisense, 5'-GTACACTTCGGAGATGGGAGTGG-3'. Data analysis was performed using Prism, and GAPDH was used as a reference transcript.

### Western blot and antibodies

Cellular proteins were extracted using RIPA buffer (Beyotime, Shanghai, China) containing a complete protease inhibitor mixture (Roche, Mannheim) and BCA method for protein concentration determination. Gel electrophoresis then transfer to a membrane. The antibodies utilized in this study included $\beta$-actin (Bioss), LC3II (Abcam), P62 (Abcam), BMAL1 (Cell Signaling Technology), STX17 (Proteintech), SNAP29 (Proteintech), and VAMP8 (Proteintech). Immunopure goat anti-rabbit and anti-mouse IgG (HL) were procured from ABclonal. The intensity of the bands was quantified using NIH ImageJ software.

### Immunoprecipitation (Co-IP)

Ice-cold immunoprecipitation buffer (50 mM Tris-HCl, pH 8.0, 150 mM NaCl, 2 mM EDTA, 10% glycerol, and 1% Triton X-100) supplemented with protease inhibitors was used to lyse the collected HT22 cells. The lysates were transferred to 1.5 ml tubes, gently rotated for 2 hours at $4^\circ$C, and then centrifuged at 13,000 rpm for 25 minutes. The supernatants were collected and incubated with either control IgG (Santa Cruz Biotechnology) or antibodies specific for STX17 (Proteintech) or SNAP29 (Proteintech) for immunoprecipitation. Protein A+G agarose beads (20 $\mu$l, Beyotime, P2012) were added to the immunoprecipitation mixture, and the mixture was gently rotated for 4 hours at $4^\circ$C. The antigen–antibody complexes were then precipitated by a brief centrifugation.

After four washes with immunoprecipitation buffer, the pellet was resuspended in SDS loading buffer and then denatured at $100^\circ$C for 30 minutes before electrophoresis.

### Immunofluorescence staining

Cells cultured on coverslips were fixed with 4% paraformaldehyde for 15 minutes. The fixed cells were washed three times and then permeabilized with 0.1% Triton X-100 for 10 minutes. After three washes, the cells were blocked with 1% bovine serum albumin (BSA) for 2 hours at $4^\circ$C. The above operations were all performed at room temperature (RT). Subsequently, the cells were incubated with light chain 3 (LC3) (rabbit), STX17 (rabbit), VAMP8 (mouse), and BMAL1 (rabbit) antibodies overnight at $4^\circ$C. The cells were

washed three times and then incubated with the corresponding secondary antibodies at RT in the dark for 2 hours. Alexa Fluor 594-conjugated anti-rabbit IgG (red) was used for STX17, while Alexa Fluor 488-conjugated anti-mouse IgG (green) was used for VAMP8. Alexa Fluor 488-conjugated anti-rabbit IgG (green) was utilized for LC3, STX17, and BMAL1. Following three washes, the nuclei were counterstained using 4',6-diamidino-2-phenylindole (DAPI) (Beyotime, C1005) for 1 minute. After the sections were sealed with mounting medium, a laser scanning confocal microscope (Olympus) was used to obtain immunofluorescence images.

### Locomotor activity measurement

Animals were randomly divided into two groups: one group remained sedentary with locked running wheels, while the other group had voluntary access to mobile running wheels for a period of 4 weeks. The animals experienced a 12-hour light/12-hour dark cycle for the initial 2 weeks, followed by 2 weeks of continuous darkness. Typically, 4-month-old mice were individually housed in cages equipped with running wheels, which were placed inside light-tight boxes with individual lighting. During the light phase, the mice were exposed to approximately 150 lux of white light from fluorescent sources. Wheel running activity was continuously recorded at 1-minute intervals and later analyzed using Clocklab software (Actimetrics, Evanston, IL, USA). All standard animal care procedures conducted during the dark phase were carried out under dim red light.

### Luciferase reporter assay

To perform dual luciferase analysis, approximately $1 \times 10^5$ HT22 cells were plated in 24-well plates. Each well was transfected with 400 ng of luciferase reporter plasmid and 2 ng of the internal control plasmid pRL-CMV vector (Jikai, China) using Lipofectamine 3.0. After 24 hours, the cells were further transfected with either the puro or puro-BMAL1 plasmid for an additional 24 hours. Subsequently, the cells were harvested and lysed using passive lysis buffer (Promega), and the luciferase activity was measured following the protocol of the dual luciferase assay system (Promega).

### QUANTIFICATION AND STATISTICAL ANALYSIS

All assays were repeated at least three times, and continuous variables that conformed to the normal distribution are presented as the mean $\pm$ SD. The comparison between the two groups was performed using the t test, and one-way repeated measures analysis of variance was used to compare multiple groups. We used GraphPad Prism curve comparisons or SPSS 22.0 to analyze the data. A value of $P < 0.05$ was considered to indicate statistical significance. The statistical details of experiments can be found in the figure legends, figures, results. In animal experiments, n represents the number of animals, but in cell experiments, n represents the number of cell sample repetitions.